

Dynamics of the Intertropical Convergence Zone of the East Pacific

DAVID J. RAYMOND

New Mexico Institute of Mining and Technology, Socorro, New Mexico

CHRISTOPHER S. BRETHERTON

University of Washington, Seattle, Washington

JOHN MOLINARI

The University at Albany, State University of New York, Albany, New York

(Manuscript received 12 May 2004, in final form 12 June 2005)

ABSTRACT

The dynamical factors controlling the mean state and variability of the east Pacific intertropical convergence zone (ITCZ) and the associated cross-equatorial boundary layer flow are investigated using observations from the East Pacific Investigation of Climate (EPIC2001) project. The tropical east Pacific exhibits a southerly boundary layer flow that terminates in the ITCZ. This flow is induced by the strong meridional sea surface temperature (SST) gradient in the region. Away from the equator and from deep convection, it is reasonably well described on a day-to-day basis by an extended Ekman balance model. Variability in the strength and northward extent of this flow is caused by variations in free-tropospheric pressure gradients that either reinforce or oppose the pressure gradient associated with the SST gradient. These free-tropospheric gradients are caused by easterly waves, tropical cyclones, and the Madden–Julian oscillation.

Convergence in the boundary layer flow is often assumed to be responsible for destabilizing the atmosphere to deep convection. An alternative hypothesis is that enhanced total surface heat fluxes associated with high SSTs and strong winds act to produce the necessary destabilization. Analysis of the moist entropy budget of the planetary boundary layer shows that, on average, surface fluxes generate over twice the destabilization produced by boundary layer convergence in the east Pacific ITCZ.

1. Introduction

The intertropical convergence zone (ITCZ) is marked by a near-equatorial, east–west band of deep convection that girdles the globe. After many years of study, we are still uncertain as to the mechanisms governing the occurrence, location, and variability of the ITCZ.

During September and October 2001 the East Pacific Investigation of Climate 2001 (EPIC2001) field program took place in the tropical east Pacific south of Mexico. Among other things, this project studied ITCZ convection and the conditions surrounding its formation and variability in the vicinity of 95°W. The longi-

tude was chosen to coincide with the 95°W line of the Tropical Atmosphere Ocean (TAO) array moorings (Hayes et al. 1991; McPhaden 1995) so that coordinated measurements could be made with this array.

Observations show that a strong cross-equatorial southerly flow exists in the east Pacific boundary layer during boreal summer and fall (Yin and Albrecht 2000). The east Pacific ITCZ is found at the northern terminus of this flow, suggesting a relationship between the two. The flow itself is driven in large part by pressure gradients associated with the meridional sea surface temperature (SST) and boundary layer air temperature gradients in this region (McGauley et al. 2004, hereafter MZB).

Since the ITCZ manifests itself most obviously by its association with convection and rainfall, it is intimately tied up with the factors controlling deep convection in the Tropics. Lindzen and Nigam (1987), Battisti et al. (1999), and others, using ideas first put forth by Riehl et

Corresponding author address: Dr. David Raymond, New Mexico Tech, 801 Leroy Place, Socorro, NM 87801.
E-mail: raymond@kestrel.nmt.edu

al. (1951), have developed models that basically assume Ekman balance in the boundary layer (pressure gradient plus Coriolis force plus drag equals zero) from which the boundary layer wind can be inferred. They further hypothesize that deep convection occurs in the Tropics where their models predict convergence in the boundary layer flow. This constitutes a dynamical model of convective forcing.

Tomas et al. (1999, hereafter THW) applied a similar model specifically to the cross-equatorial flow in regions with strong latitudinal SST gradients, such as the east Pacific. This model differs from those of Lindzen and Nigam (1987) and Battisti et al. (1999) in that it includes the meridional advection of zonal and meridional momentum in the momentum balance as well as a different treatment of the geopotential.

To close models of this type, some empirical relation between sea level pressure and SST must be postulated. This closure assumption implicitly substitutes for a thermodynamic closure on tropical oceanic convection. In this sense, these dynamical models are incomplete.

Stevens et al. (2002) extended the Ekman balance idea to include the contribution to the momentum balance of the boundary layer of air entrained from above. MZB tested this model against EPIC2001 observations and found that it gave good agreement with the time-averaged boundary layer flow.

A different perspective is gained by considering the primary control on convection to be local thermodynamics. For instance, Raymond et al. (2003, hereafter R03) established that roughly two-thirds of the variance in infrared brightness temperature over a $4^\circ \times 4^\circ$ square centered at 10°N , 95°W can be explained by a combination of variations in the mean moist entropy flux from the ocean and a measure of the convective inhibition, with the variations in entropy flux being responsible for most of the variance. These results are based on the boundary layer quasi-equilibrium ideas of Raymond (1995) and favor a more thermodynamically based model for convective forcing in the east Pacific ITCZ.

Other evidence shows that deep convection is sensitive to variations in the relative humidity of the atmosphere, particularly in regions such as Kwajalein, Marshall Islands, which lies near the edge of the moist tropical belt (e.g., Bretherton et al. 2004). Further work by Back and Bretherton (2005) finds that convection throughout the tropical Pacific is independently sensitive to free tropospheric humidity and surface wind speed, the latter of which is presumably acting as a surrogate for surface moist entropy flux. The independent sensitivity of convection to these quantities supports a model in which boundary layer quasi equi-

librium controls the amount of convection and the free-tropospheric humidity controls its precipitation efficiency. Three independent factors thus control precipitation in this picture: surface entropy fluxes, convective inhibition, and free-tropospheric humidity.

In this paper we use observations from EPIC2001 augmented by the Quick Scatterometer (QuikSCAT) winds and other satellite data to examine how the above ideas play out in the east Pacific ITCZ. In particular, we investigate whether MZB's model is able to reproduce day-to-day variability of the boundary layer meridional wind as well as its time average. Finally, we determine how well this model is able to predict the location of deep convection in this region relative to boundary layer quasi equilibrium.

Section 2 briefly describes the EPIC2001 project while section 3 reviews the theoretical basis of the Ekman balance and related models, as well as boundary layer quasi equilibrium. Section 4 documents the mean state of the atmosphere in the ITCZ region, while section 5 discusses the factors controlling convective variability there. Conclusions are presented in section 6 while the appendix presents details on the calculation of pressure gradients from airborne data.

2. EPIC2001

In this section we present a brief description of the EPIC2001 observational tools used in this paper. R03 and Raymond et al. (2004, hereafter R04) provide more detailed information on this project.

Figure 1 shows the experimental region. Two flight patterns of particular interest to this paper are the 95°W traverses of the National Center for Atmospheric Research's C-130 aircraft and the ITCZ missions of the National Oceanic and Atmospheric Administration's P-3. In the former, the C-130 flew from 12°N to 1°S along 95°W , alternating between altitudes of 30 and 1600 m, allowing both altitudes to be sampled. The aircraft returned at 6300 m, deploying dropsondes at 1° intervals. Eight such missions were flown and their dates are listed in R03.

The P-3 flew 10 ITCZ missions (dates in R03) in which a $4^\circ \times 4^\circ$ grid pattern was flown at an elevation of 1900 m. This pattern was centered on 10°N , 95°W . Dropsondes were deployed every 1° – 2° , allowing the flow and thermodynamics of the region to be mapped. In addition, the P-3's X-band Doppler radar was run continuously in "FAST" mode using a dual pulse rate technique to mitigate Doppler velocity ambiguities (Jorgensen et al. 1996, 2000).

The static pressure and radar altimeter data were used to deduce pressures at a fixed level near the air-

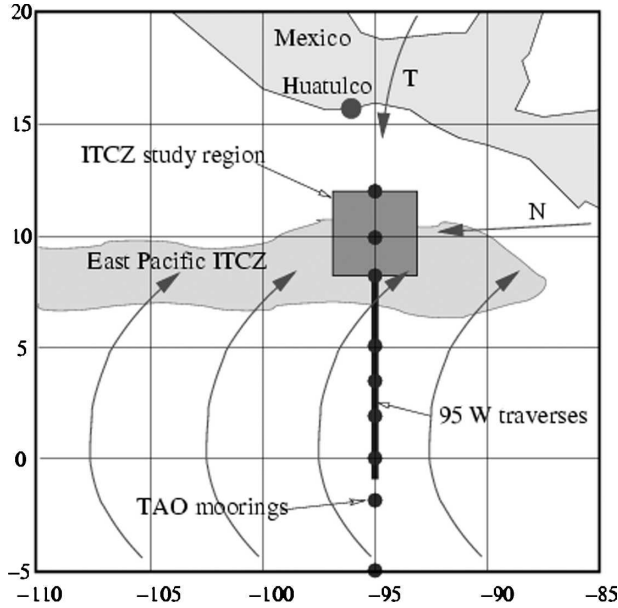


FIG. 1. Map of the eastern tropical Pacific showing the ITCZ, general surface flows, locations of TAO moorings and the ITCZ study region, and the aircraft base in Huarulco, Mexico. (Reproduced from R03.)

craft flight level for both C-130 and P-3 aircraft. The technique used to do this is described in the appendix.

3. Theoretical basis

In this section we develop the theoretical basis needed to evaluate both the dynamic and thermodynamic hypotheses for the origin and variability of the east Pacific ITCZ. We first review the model of MZB and show how the THW's model is related to it for the case in which the zonal boundary layer wind is determined from observation. We then develop a slightly extended model of boundary layer quasi equilibrium (BLQ) in which the ideas of Raymond (1995) are applied to the full planetary boundary layer (PBL: the layer from the surface to the tops of shallow convective clouds) rather than just the subcloud layer.

a. MZB's model

MZB showed that an extended Ekman balance model was able to predict the time-averaged southerly PBL flow south of the ITCZ in the eastern Pacific. Ekman balance is a local balance between the pressure gradient force, the Coriolis force, and surface friction. The extension to the model was developed by Stevens et al. (2002) and consists of adding to the list of forces the momentum source associated with the entrainment of free-tropospheric air into the PBL from above. MZB

showed that this term is the same order of magnitude as the other terms in the momentum balance in the tropical east Pacific boundary layer flow.

The equations for the zonal and meridional momentum balance in the extended Ekman balance model are

$$\frac{du}{dt} = -\frac{1}{\rho} \frac{\partial p}{\partial x} - \frac{C_d}{h} (u^2 + v^2)^{1/2} u + fv + \frac{(u_t - u)w_s}{h} = 0, \quad (1)$$

$$\frac{dv}{dt} = -\frac{1}{\rho} \frac{\partial p}{\partial y} - \frac{C_d}{h} (u^2 + v^2)^{1/2} v - fu + \frac{(v_t - v)w_s}{h} = 0, \quad (2)$$

where (u, v) is the boundary layer wind, (u_t, v_t) is the wind at the top of the boundary layer, p and ρ are the pressure and density in the boundary layer, and w_s is the subsidence velocity at the top of the boundary layer. In addition we have the Coriolis parameter as a function of latitude f , the drag coefficient C_d , and the effective depth of the mixed layer h . We take $C_d = 0.0011$, $h = 500$ m, and $w_s = 0.01$ m s⁻¹ after MZB and obtain (u, v) from low-level C-130 in situ measurements, taken typically 30 m above the surface, and (u_t, v_t) from C-130 in situ measurements near 1000 m.¹ The pressure is extrapolated hydrostatically to the surface from the low-level values, as described in the appendix. Sample values measured at each level as the C-130 passed through the desired level in its porpoising maneuvers between 30 and 1600 m are interpolated and smoothed to obtain a continuous record at each level of interest.

MZB solved the equations with the zonal pressure gradient obtained from reanalysis data. We employ a slightly different approach. The zonal wind is measured for each of these flights, so we take this as known and treat the meridional PBL wind and zonal pressure gradient as unknowns. The meridional wind computed from solving (2) is then compared with observation and used with (1) to solve for the zonal pressure gradient. In this context the MZB's model is actually quite close to the THW's model in that exploration of the factors governing the zonal wind and the latitudinal pressure distribution is sidestepped. There are only two remaining differences between the two theories when the zonal wind and pressure distributions are taken as known: MZB includes entrainment of free-tropospheric momentum, while THW includes the meridional advection of meridional momentum. Scaling arguments sug-

¹ Note that the value of h chosen by MZB is much less than the depth of the full PBL. This reflects the less-than-well-mixed nature of the PBL.

gest that the meridional advection term is not of primary importance away from the equator, so we confine our calculations to MZB's model.

b. BLQ extended

The boundary layer quasi-equilibrium model of Raymond (1995) examined the moist entropy budget in the subcloud layer. This layer was assumed to be well mixed in moist entropy. The two most important contributors to the entropy budget were assumed to be surface moist entropy fluxes (positive) and convective downdrafts (negative). Variations in the boundary layer entropy result in corresponding variations in convective available potential energy (CAPE) and convective inhibition (CIN). Thus, if surface fluxes increase, the boundary layer entropy and CAPE increase and CIN decreases. The decrease in CIN in particular is hypothesized to result in more convective updrafts and hence more downdrafts. Eventually, the surface and downdraft fluxes should reach a new equilibrium corresponding to a state with increased convection. A decrease in surface fluxes should result in a corresponding decrease in convection. In this way the surface moist entropy flux is thought to control the amount of convection via its effect on the convective inhibition. If for some reason the convective inhibition is very strong, then the above feedback loop is broken, and there is simply no convection outside of the PBL.

R03 evaluated the moist entropy budget in a control volume in the east Pacific consisting of the $4^\circ \times 4^\circ$ square with the top set by the elevation of 1900 m flown by the P-3 aircraft during the ITCZ missions. This elevation is just above the top of the PBL, that is, the layer consisting of the subcloud region plus boundary layer clouds. The PBL is much less homogeneous than the subcloud layer, and this inhomogeneity needs to be taken into account in a modified theory of BLQ applied to the PBL.

The budget equation for perturbation moist entropy $s' = s - s_R$ as given by R03 is

$$\frac{ds'}{dt} = \frac{g\overline{F}_s}{\Delta p} + \overline{R}_s - \frac{P\langle s'u_n \rangle}{A} - \frac{g\rho\overline{s'w}}{\Delta p}, \quad (3)$$

where the budget is applied to a volume of pressure depth Δp , area A , and perimeter P . An underbar indicates a volume average, an overbar means an areal average, and angle brackets indicate an average over the lateral faces of the volume. The acceleration of gravity is g , F_s is the surface entropy flux, R_s is the radiative source of entropy, u_n is the outward normal air velocity component on the lateral faces, and w and ρ are the vertical velocity and air density at the top of the volume.

The constant reference entropy s_R is set to the mean entropy of updraft air exiting the top of the volume:

$$s_R = \overline{sw'_u/w'_u}, \quad (4)$$

where $w'_u = w$ for $w > 0$ and zero for $w < 0$. The particular choice of s_R does not affect the validity of the entropy budget. However, it is important for our interpretation of the budget: updraft air does not contribute, and the balance is thus between surface fluxes, radiation, lateral inflow/outflow, and downdraft fluxes through the top of the volume. The downdraft fluxes can therefore be expressed uniquely in terms of quantities that are thought to force deep convection, surface fluxes, and imposed convergence in particular.

Raymond (1995) assumed, in addition, that the mean entropy of air flowing laterally through the walls of the control volume differed insignificantly from s_R , which means that the lateral flow term could be ignored. This assumption is less likely to be true in the full PBL than in the subcloud layer. Thus, we need to include the contribution of lateral inflow to the moist entropy budget in the PBL. The fraction of the total entropy source due to horizontal convergence indicates the relative importance of boundary layer convergence to surface fluxes in supporting tropospheric deep convection.

R03 also developed an index for convective inhibition (DCIN) based on the mean buoyancy of a layer consisting of (roughly) the lowest 100 hPa of the atmosphere:

$$\text{DCIN} = s_t - s_b, \quad (5)$$

where s_b is the moist entropy in this layer and s_t is the saturated moist entropy in a layer just above the PBL. This was assumed to be centered near 820 hPa for convenience, as the P-3 aircraft flew all of its missions at this level. DCIN was thought to be more appropriate for the control of deep convection than indices based on subcloud conditions since in-cloud measurements of updrafts in deep convection over the east Pacific were invariably found to consist of a mixture of air from the entire PBL rather than from just the subcloud layer. This is the primary reason we wish to apply BLQ to a deeper layer than was contemplated by Raymond (1995).

The entropy balance in the PBL governs the downdraft entropy flux into the PBL according to the above theory. Free-tropospheric environmental conditions presumably control the form of the convection resulting from the ascent of PBL air and, in particular, the ratio of updraft mass flux to downdraft entropy flux. The larger this ratio, the greater will be the updraft mass flux for a given amount of surface flux forcing. Thus, for a complete picture of convective forcing, we must in-

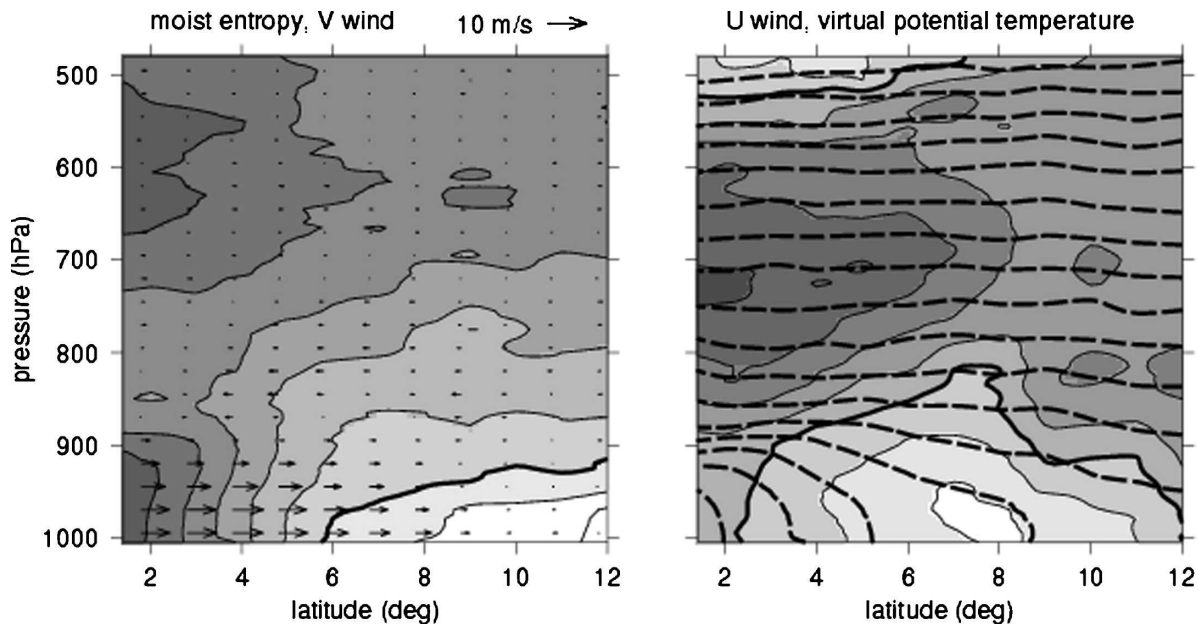


FIG. 2. (left) Mean moist entropy (contours and shading, $10 \text{ J kg}^{-1} \text{ K}^{-1}$ intervals, heavy contour at $240 \text{ J kg}^{-1} \text{ K}^{-1}$, lighter shades indicating higher values) and meridional wind vectors. (right) Mean zonal wind (solid contours and shading, 2 m s^{-1} contour interval, darker more easterly, thick contour shows zero value) and virtual potential temperature (dashed contours at 2-K intervals). All from C-130 dropsondes deployed along 95°W .

investigate the effect of free-tropospheric conditions on convection.

Aside from the existence of CAPE, which is rarely an issue over warm tropical oceans, the single most important factor controlling deep convection in the free troposphere appears to be tropospheric humidity. Observational (Sherwood 1999; Sobel et al. 2004; Bretherton et al. 2004) and modeling (Lucas et al. 2000; Tompkins 2001; Grabowski 2003; Raymond and Zeng 2005) studies show that deep convection is, in fact, quite sensitive to the tropospheric relative humidity. Bretherton et al. (2004) indicate that the ratio of precipitable water to saturated precipitable water (which we denote *saturation fraction*) is perhaps the most compact variable with which to represent this sensitivity.

4. The mean state of the ITCZ

To gain an understanding of east Pacific ITCZ dynamics, we first document the kinematics of the mean ITCZ. We then examine the relative importance of PBL convergence and the surface entropy flux in forcing the observed convection.

A number of observations have documented the low-level, cross-equatorial flow in the eastern Pacific that occurs during the northern summer and fall (e.g., Yin and Albrecht 2000). These show a persistent southerly flow at the equator, turning to southwesterly as it moves to the north. The flow is about 1 km deep.

Figure 2 shows the mean moist entropy and meridional flow from 1.5° to 12°N from dropsondes deployed on the eight C-130 flights traversing 95°W . The northward increase in low-level moist entropy is evident as the southerly flow passes over warmer SSTs. A broad maximum in moist entropy occurs above 800 hPa north of 6°N , with lower values to the south. The northerly return flow near 800–850 hPa is seen in other observations taken in this region as well (Zhang et al. 2004).

Figure 2 also shows the mean zonal wind from the eight C-130 flights as well as contours of the virtual potential temperature. Below 850 hPa the air is colder to the south, as is to be expected from the SST distribution. Above this level the meridional gradients of virtual potential temperature are weak. The low-level westerly winds peak near 8°N .

Figure 3 shows averages as a function of latitude over the eight C-130 95°W flights of a wide variety of fields. We note that the sea surface temperature increases monotonically from the equator to at least 12°N and, in fact, is maximal at the Mexican coast. In spite of this, the lowest infrared brightness temperature occurs at 8°N , implying a maximum in deep convection at this latitude, a fact noted by Tomas and Webster (1997) and THW.

In our sample of C-130 dropsondes, the maximum average surface wind speed is about 8 m s^{-1} near 4°N . Note that the difference between two estimates of the

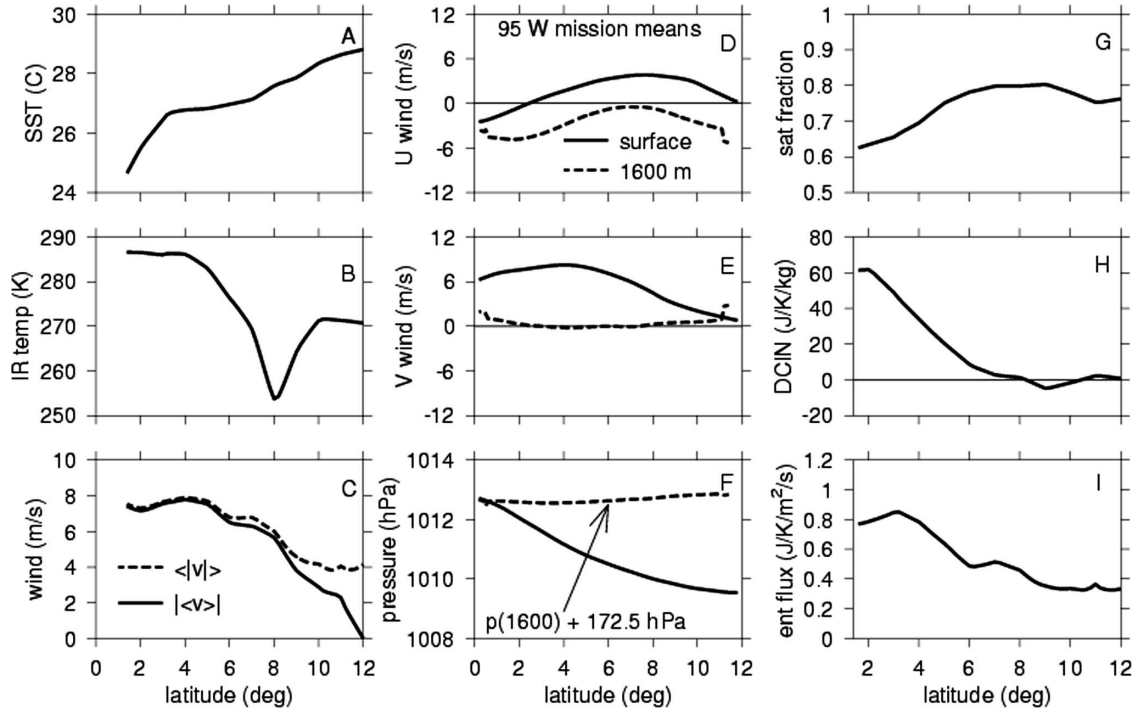


FIG. 3. Quantities along 95°W averaged over the C-130 95°W flights: (a) Reynolds (Reynolds 1988; Reynolds and Marsico 1993) SST averaged over 93°–97°W and over the period of the field program, (b) infrared brightness temperature along 95°W during the C-130 flights (solid line) and averaged over 93°–97°W and over the period of the field program (dashed line). (c) Low-level (980–1000 hPa) dropsonde wind speed computed in two ways: the average of the magnitude of the vector wind (dashed line) and the magnitude of the average of the vector wind (solid line). Surface and 1600-m (d) zonal winds and (e) meridional winds from C-130 in situ observations. (f) Pressure at surface and 1600 m from the C-130. The 1600-m pressure curve is offset so that the pressure at the two levels can be shown on the same graph. (g) Saturation fraction below 480 hPa, and (h) DCIN and (i) surface moist entropy flux calculated from C-130 dropsondes.

mean wind speed, $\langle |\mathbf{v}| \rangle$ and $|\langle \mathbf{v} \rangle|$, where the angle brackets indicate an average over the eight C-130 flights, is insignificant south of 8°N, but increases rapidly north of this latitude. This indicates increasing variability in wind direction as one moves north. At 12°N $|\langle \mathbf{v} \rangle|$ is essentially zero, whereas $\langle |\mathbf{v}| \rangle$ is roughly 4 m s⁻¹ north of 9°N.

The middle column in Fig. 3 shows the wind and pressure at two different heights, the surface and 1600 m, as derived from C-130 in situ data during the 95°W missions. The pressures were reduced to standard heights using radar altimeter data and the hydrostatic equation, as described in the appendix. The latitudinal variation of the difference between the surface and 1600-m pressures reflects the increase in the virtual temperature of the air from 0° to 12°N.

Interestingly, the mean meridional pressure gradient at 1600 m is very weak, which means that the surface pressure gradient driving the mean low-level meridional flow is due on the average almost totally to the temperature gradient of PBL air and, hence, of the ocean surface. Nearly uniform easterly shear of about

5 m s⁻¹ exists in the mean between the surface and 1600 m, and surface westerlies are found from 2°N to 12°N with a maximum near 8°N.

Zonal structure in this region is associated primarily with traveling wave disturbances. Since Fig. 3 represents an average over all 95°W missions, this zonal structure is likely to be averaged out to a significant degree, which means that the total convergence should be adequately represented by the averaged meridional convergence.

The meridional surface wind shown in Fig. 3 decreases monotonically from 4° to 12°N, implying meridional surface mass convergence over this full latitude range. The strong negative peak in infrared brightness temperature occurs in the middle of this range at 8°N. Thus, the actual convection is more focused in latitude than the surface convergence.

The right-hand column of plots in Fig. 3 shows time-mean values of the saturation fraction below 500 hPa, the DCIN, and the surface moist entropy flux F_s . The surface moist entropy flux is estimated using a simple bulk formula:

$$F_s = \rho_s C_d U_s (s_{ss} - s_s), \quad (6)$$

where $\rho_s = 1.2 \text{ kg m}^{-3}$ and U_s and s_s are the wind and moist entropy, averaged in dropsonde data over 980–1000 hPa, and s_{ss} is the saturated moist entropy at the sea surface temperature and pressure.

Surface entropy fluxes actually maximize at low latitudes, but DCIN is too large to support deep convection in this region due to the low values of PBL moist entropy. DCIN becomes small as the moist entropy of the PBL increases and the saturation fraction reaches 0.8 near 7°N, which marks a strong increase in deep convection according to the infrared brightness temperature plot in Fig. 3. Surface fluxes weaken slightly and the saturation fraction decreases north of 9°N, which coincides on the average with less deep convection. Thus, the distribution of deep convection with latitude, seen in Fig. 3, is consistent with the hypothesis that convection is controlled by convective inhibition and tropospheric saturation fraction.

Figure 4 shows the results of the MZB's model applied to the average of the eight C-130 flights. The calculated meridional surface wind is in good agreement with observation in this case. The theory agrees less well with observation when the entrainment of momentum from subsiding air is neglected, as indicated by MZB.

The middle panel in Fig. 4 shows that the standard deviation of the difference between observed and computed meridional wind is about 2 m s^{-1} south of 7°N, but increases to as much as 5 m s^{-1} north of this latitude. We believe that this represents the effects of deep convection on the boundary layer momentum balance, which are not present in the simple Ekman balance model.

The bottom panel in Fig. 4 shows the measured meridional pressure gradient, dp/dy , and the inferred zonal pressure gradient, dp/dx . The zonal pressure gradient is much smaller than the meridional gradient, confirming the existence of near-zonal symmetry on the average.

The observations discussed above do not tell us the relative importance of PBL entropy convergence and surface moist entropy fluxes in forcing deep convection in the east Pacific ITCZ. However, the PBL moist entropy budget discussed in section 3 provides a basis for making this judgement. Table 1, which is adapted from R03, shows the mean PBL sources of moist entropy in the east Pacific ITCZ. Averaged over the ten P-3 flights in the ITCZ study region, lateral entrainment provides $7.5 \text{ J K}^{-1} \text{ kg}^{-1} \text{ day}^{-1}$, or 29% of the moist entropy supply to the PBL, while surface fluxes provide $18 \text{ J K}^{-1} \text{ kg}^{-1} \text{ day}^{-1}$, or 71%. Lateral entrainment thus provides less than a third of the entropy needed to balance

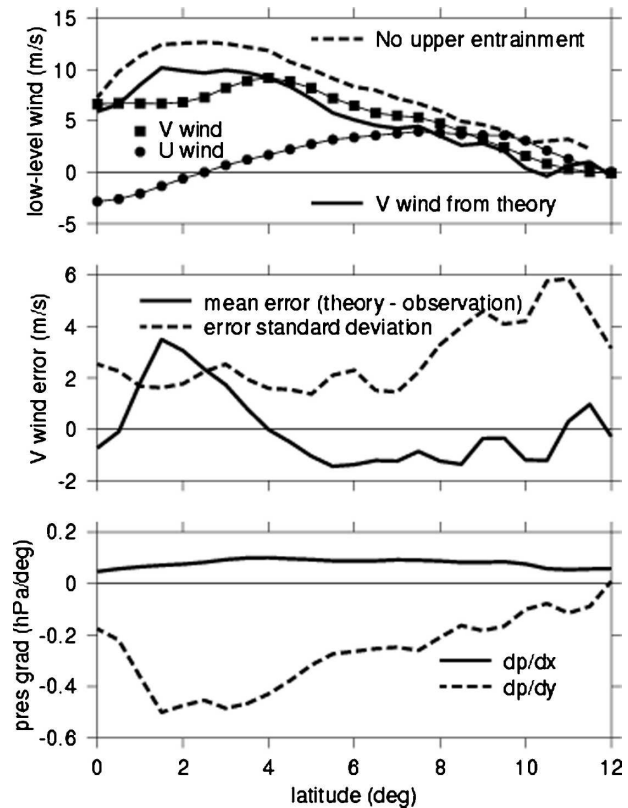


FIG. 4. Averages over the 8 C-130 flights along 95°W. (top) Observed zonal and meridional winds near the surface are shown by filled bullets and squares, respectively. The predicted meridional wind is shown by the thick solid line and the predicted meridional wind without momentum entrainment from above is given by the dashed line. (middle) The solid line shows the mean error between the observed and predicted meridional wind. The standard deviation in this error is shown by the dashed line. (bottom) The mean zonal (solid line) and meridional (dashed line) pressure gradients at the surface are illustrated.

the negative tendencies induced by downdrafts and radiative cooling, whereas surface fluxes provide more than two-thirds. Therefore, PBL convergence (which is primarily responsible for the lateral entrainment) apparently plays a relatively minor role in forcing deep convection in the region, whereas surface fluxes provide the lion's share of the forcing.

5. ITCZ variability

We first display the general features of subseasonal ITCZ variability in the east Pacific, which we find to be due primarily to the passage of easterly waves and the Madden-Julian oscillation (MJO). We then examine two cases studies in some detail: one with enhanced convection and the other with suppressed convection.

TABLE 1. Volume-mean contributions to the moist entropy budget of the ITCZ study region below 1900 m from surface and lateral fluxes. The budgeted quantity is actually the moist entropy minus the mean moist entropy in updrafts out of the top of the volume. The right column gives the mean rainfall rate determined from P-3 radar observations. (Results adapted from R03.)

Mission	Surface flux ($\text{J K}^{-1} \text{kg}^{-1}$ day^{-1})	Lateral flux ($\text{J K}^{-1} \text{kg}^{-1}$ day^{-1})	Rain rate (mm day^{-1})
1	15.3	6.3	—
2	21.1	4.1	6.7
4	30.7	9.8	18.0
5	12.9	7.1	7.0
7	20.2	3.0	14.4
9	18.1	9.1	10.8
15	16.2	8.6	6.0
16	11.6	9.1	4.3
17	18.8	12.8	12.2
18	15.1	5.5	4.8
Mean	18.0	7.5	9.4

The relative contributions of entropy convergence and surface fluxes are determined.

a. General features of ITCZ variability

Figure 5 shows the infrared brightness temperature in the range 8° – 12°N as a function of longitude and time during the field phase of EPIC2001. It is evident that the bulk of the variability in deep convection resulted from the passage of westward-moving disturbances during the project.

Figure 6 shows the convective structure as a function of latitude and time. Days with weak convection often have the convection concentrated near 8° – 9°N . However, on strongly convective days the convection is distributed much more broadly in latitude, with many events ranging from 6° to 13°N or greater.

Figure 7 shows a time series of observations from the EPIC2001 project. Aircraft observations at 810–830 hPa in the ITCZ study region indicate that the zonal wind at this level is very nearly geostrophic in spite of its proximity to the equator. Pulses of westerlies are accompanied by enhanced deep convection and tropical cyclogenesis. These pulses are correlated with stronger than average surface wind speeds, in agreement with the hypothesis of R03 that strong, areally averaged, surface fluxes are associated with the production of deep convection. The zonal wind at 810–830 hPa shows a change near day 274, with the wind shifting from alternating easterlies and westerlies to a much stronger easterly regime.

The stronger surface wind speeds noted above result primarily from enhanced surface southerlies. This

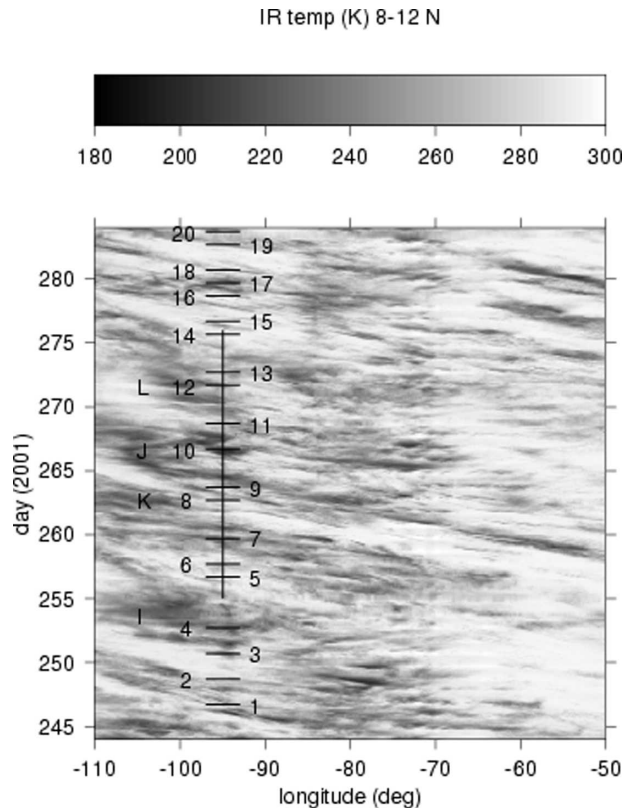


FIG. 5. GOES infrared brightness temperature averaged over 8° – 12°N as a function of longitude and day of year during EPIC2001. The numbers indicate aircraft missions and the vertical line shows the time during which the ship *Ron Brown* resided at 10°N . The letters indicate the passage of tropical storm precursors through the ITCZ study region. Day 245 is 2 Sep 2001.

makes sense from the point of view of geostrophic dynamics—westerly winds aloft are geostrophically associated with lower free-tropospheric pressure to the north. This pressure gradient reinforces the pressure gradient associated with the SST distribution, causing the surface southerlies to be stronger and extend farther to the north. We suspect that this is why westerlies just above the PBL top are associated with enhanced deep convection in the east Pacific ITCZ.

Two measures of precipitable water in the ITCZ study region are shown in the bottom panel of Fig. 7: SSM/I satellite microwave observations and dropsonde measurements. The dropsonde observations of precipitable water below 480 hPa are less than the SSM/I values, possibly because of the neglect of water vapor overlying this level. Both measurements caught the dips in precipitable water that occurred near days 256 and 263. Aside from these dips, the precipitable water varied over a relatively small range, suggesting that these variations were not a major factor in the control of precipitation during the period of the project.

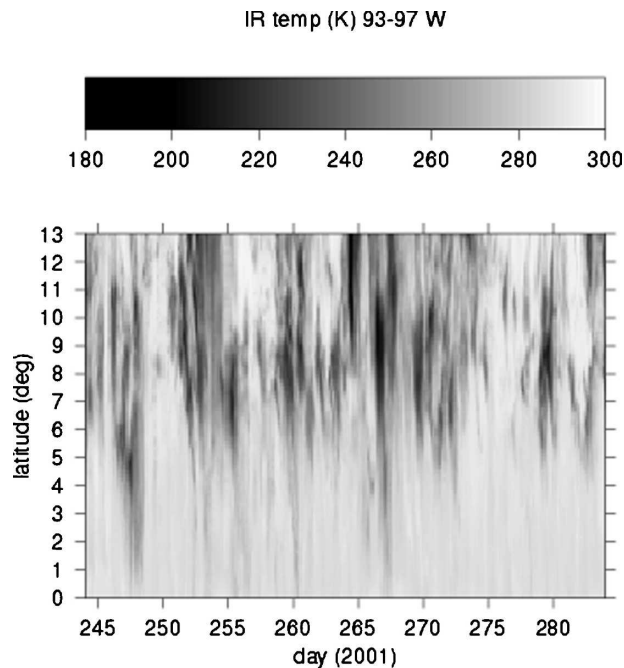


FIG. 6. Infrared brightness temperature averaged over 93° – 97° W as a function of latitude and day of year.

Figure 8 shows the conditions during summer 2001 on the global scale using the European Centre for Medium-Range Weather Forecasts 40-yr Re-Analysis (ERA-40) 2.5° pressure level analyzed winds and outgoing longwave radiation (OLR) (Liebmann and Smith 1996) data. The left panel presents the perturbation zonal wind (wind minus time average at each point) at 850 hPa while the center panel shows the OLR for the same interval and latitude range.

The OLR map of this figure indicates that EPIC2001 took place during a relatively cloudy (and presumably rainy) period in the east Pacific ITCZ. From day 263 to 275 the precipitable water was greater than average. This corresponded to the strongest convective period of the project in the ITCZ study region.

The ERA-40 analysis indicates that the period of enhanced convection coincided with westerly wind perturbations at 850 hPa. The westerlies in the east Pacific during this period appeared to arrive there via both easterly and westerly propagation from an origin in the tropical Indian Ocean. The easterly propagation across the Pacific appears to have the character of the Madden-Julian oscillation, given its scale and velocity of propagation (Madden and Julian 1994). The significance of the apparent westerly propagation across Africa and the Atlantic Ocean is unknown, and may simply be a coincidence.

Deep convection and the production of tropical cy-

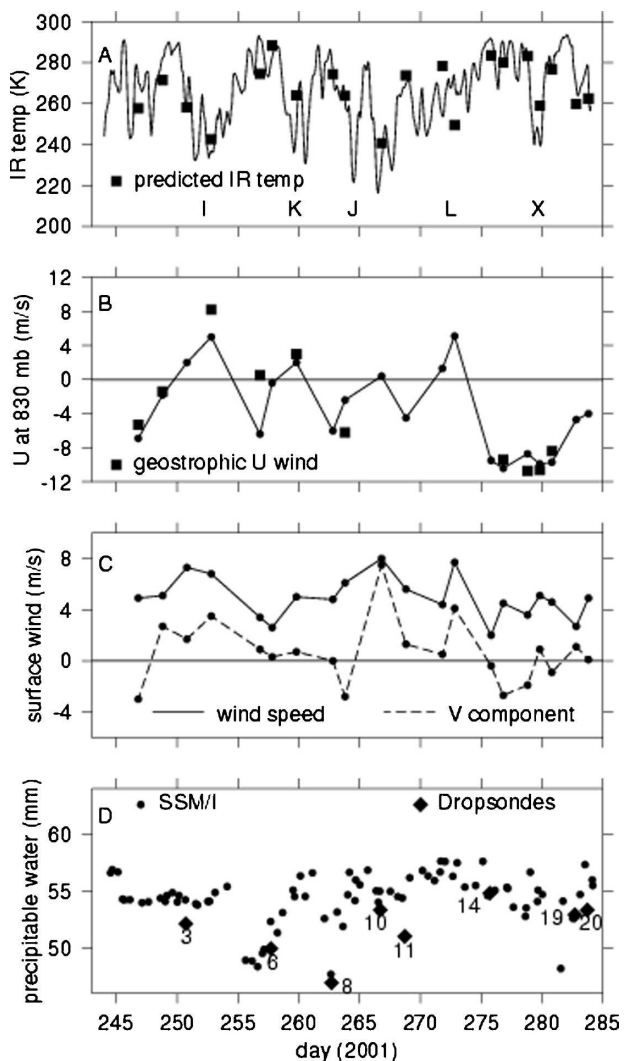


FIG. 7. Time series for EPIC. (a) Satellite infrared brightness temperature averaged over the ITCZ study region. The squares show a predicted brightness temperature based on aircraft observations (see R03). The letters I, J, K, and L represent passage of tropical storm precursors through 95° W. The letter X indicates convection apparently associated with a strong easterly jet. (b) Average zonal wind between 810 and 830 hPa from dropsondes in the ITCZ study region. The solid squares show the geostrophic zonal wind near 810 hPa from P-3 in situ pressure measurements. (c) Surface meridional and total wind averaged over the ITCZ study region. Dropsonde winds were averaged over 980–1000 hPa to obtain these results. (d) Precipitable water averaged over 8° – 12° N, 94° – 96° W from SSM/I satellite observations and dropsondes. Diamonds indicate dropsonde-measured precipitable water below 480 hPa from the C-130 95° W flights labeled with the mission number. (Reproduced in part from R04.)

clones were concentrated in the period of westerly wind perturbation. When the relative westerlies shut off near day 275, the convection decreased, as would be expected from the relationship between westerlies aloft

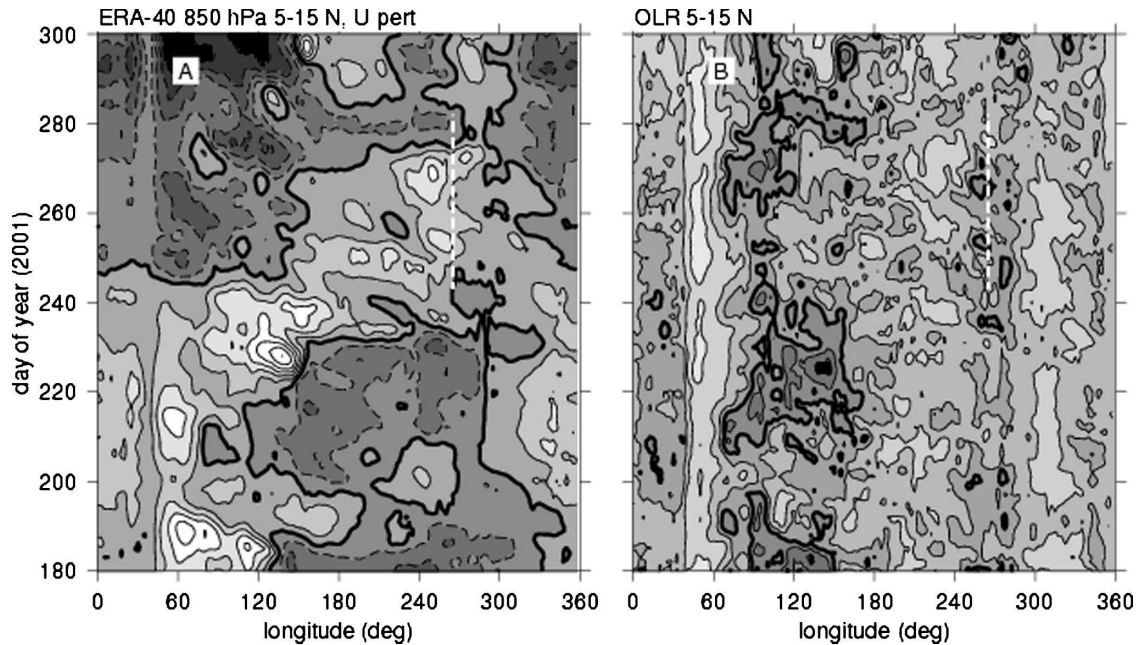


FIG. 8. ERA-40 analysis and OLR observations averaged over 5°–15°N from the end of June through the end of October 2001. (a) Perturbation zonal wind at 850 hPa, 2 m s⁻¹ contour interval, heavy line indicates zero, lighter indicates more westerly. (b) OLR, contour interval 25 W m⁻², heavy contour 200 W m⁻², lighter indicates larger values. Dashed white lines indicate dates and location of the EPIC2001 field program.

and enhanced surface southerlies. As is generally true during non–El Niño years, the signature of the MJO in the OLR is largely absent between the date line and the far east Pacific.

Table 1 provides information about the variation of surface and lateral boundary fluxes of moist entropy with the rainfall rate in the ITCZ study region. If boundary layer convergence were a significant source of deep convective forcing in this region, one might expect the fraction of the entropy supply in the PBL due to this convergence to increase on days with strong convection. However, examination of the table reveals no obvious trend in this sense, a result made amply clear by Fig. 9.

b. Case studies

In this subsection we take a closer look at the structure of the ITCZ in two cases, one with active and the other with suppressed conditions.

1) ACTIVE CONDITIONS

The most convectively active day in which a C-130 95°W mission took place was 23 September 2001 (mission 10, day 266). Figure 10 shows that the southerly flow on this day was much deeper (up to about 820 hPa)

and extended much farther north than in the mean case shown in Fig. 10. PBL zonal winds were actually westerly everywhere north of 3°N except for a convectively perturbed region between 8° and 10°N. Near 10°N westerlies extended to at least 500 hPa. Surface moist

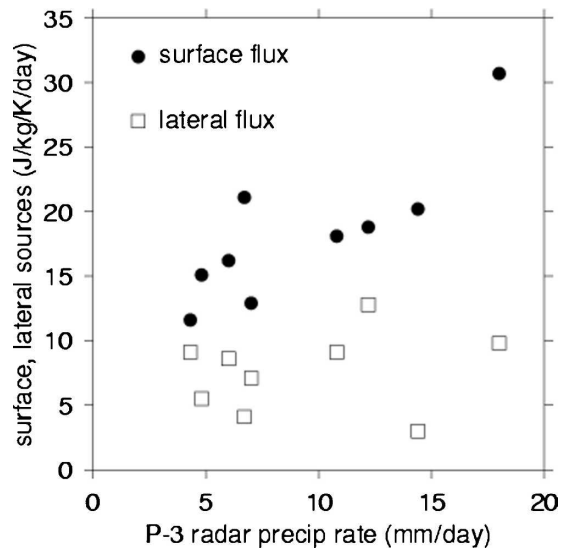


FIG. 9. Partial tendencies of moist entropy due to lateral entrainment (squares) and surface fluxes (circles) in the ITCZ study region below 820 hPa vs the P-3 radar rainfall rate.

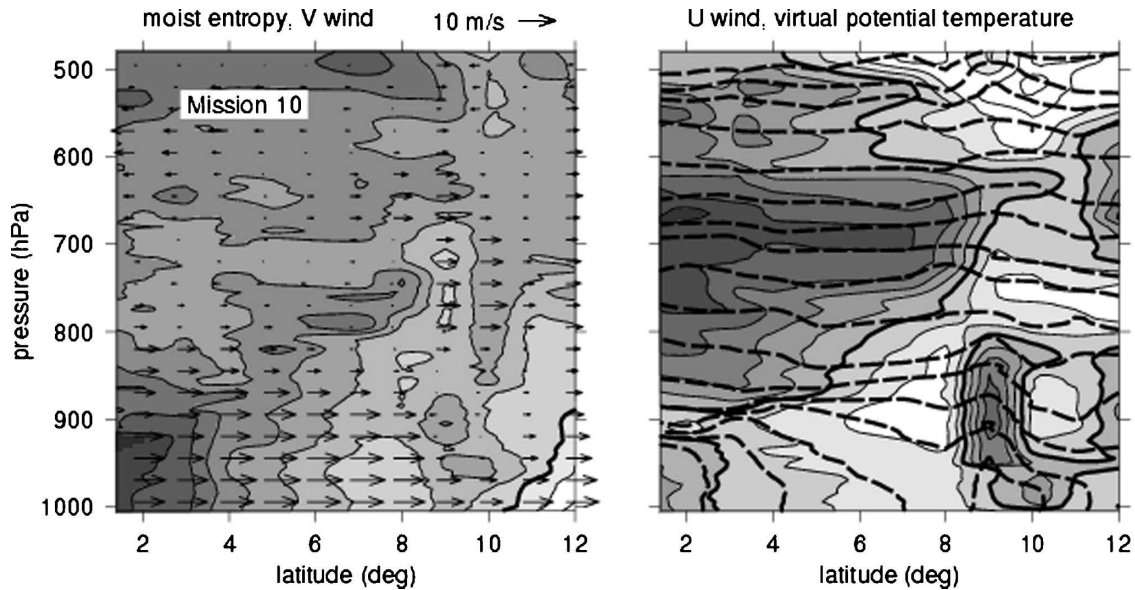


FIG. 10. As in Fig. 2, except for mission 10 (23 Sep 2001, day 266).

entropy values north of about 6°N were considerably lower than in the mean case and as a consequence the vertical gradient of moist entropy is less. This is presumably a consequence of the existence of widespread deep convection with associated downdraft production on this date.

Figure 11 shows the QuikSCAT (Freilich et al. 1994) winds and the satellite infrared brightness temperature observed on 23 September 2001. Hurricane Juliette is centered at 14°N , 101°W . The strong southerly flow experienced along 95°W is clearly part of the cyclonic circulation about this system.

If we define the ITCZ as the northern extremity of the southerly flow, its form is grossly distorted by the presence of Juliette, going from 8°N east of 90°E to near the Mexican coast (16°N) at 100°W , to 6°N near 107°W . Whether one actually wishes to refer to this interface as an ITCZ is a matter of debate. In any case, Juliette was drawing in surface air somewhat asymmetrically with the primary flows coming from the south on the southeast flank and from the northwest on the west flank.

Figure 12 shows that the surface meridional pressure gradient is significantly stronger than the mean (see Fig. 3) and that the 1600-m pressure decreases to the north as well. The difference between surface 1600 m and surface pressure increases more rapidly to the north as well, due to the warmer virtual temperatures north of 10°N (see the right panel in Fig. 10).

Figure 12 shows reasonable (but not outstanding) agreement between MZB's theory and the meridional wind up to 9°N for this case, but disagreement north of

this latitude. Significant convection occurred on this day along 95°W over the range 8° – 11°N , and observation shows that significant low-level convergence coincided with this convection. However, MZB's theory does not predict the convergence, so it cannot be said to have predicted the convection.

The saturation fraction is higher than in the mean

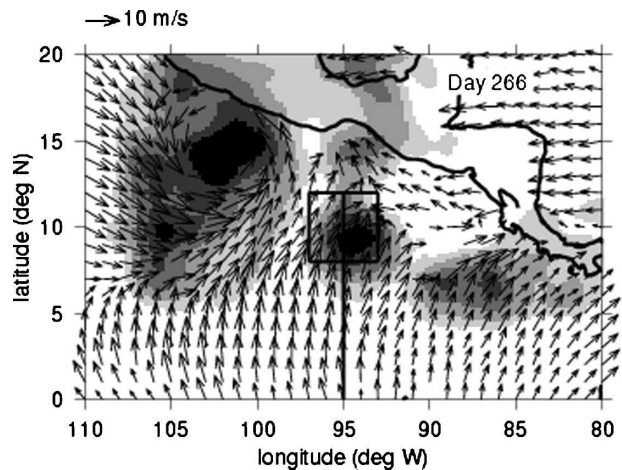


FIG. 11. Satellite infrared brightness temperature (shading contour interval 10 K, suppressed warmer than 260 K) and QuikSCAT surface winds for mission 10 (23 Sep 2001, day 266). Winds are objectively analyzed to a 1° grid with a 0.5° radius of influence. Both ascending and descending branch data are included in the analysis, but data with the rain flag set are omitted. The brightness temperature is averaged over a day and smoothed with a 0.5° low-pass filter. Thick lines show the ITCZ study region, the track followed by the C-130 along 95°W , and the coastline of Mexico and Central America.

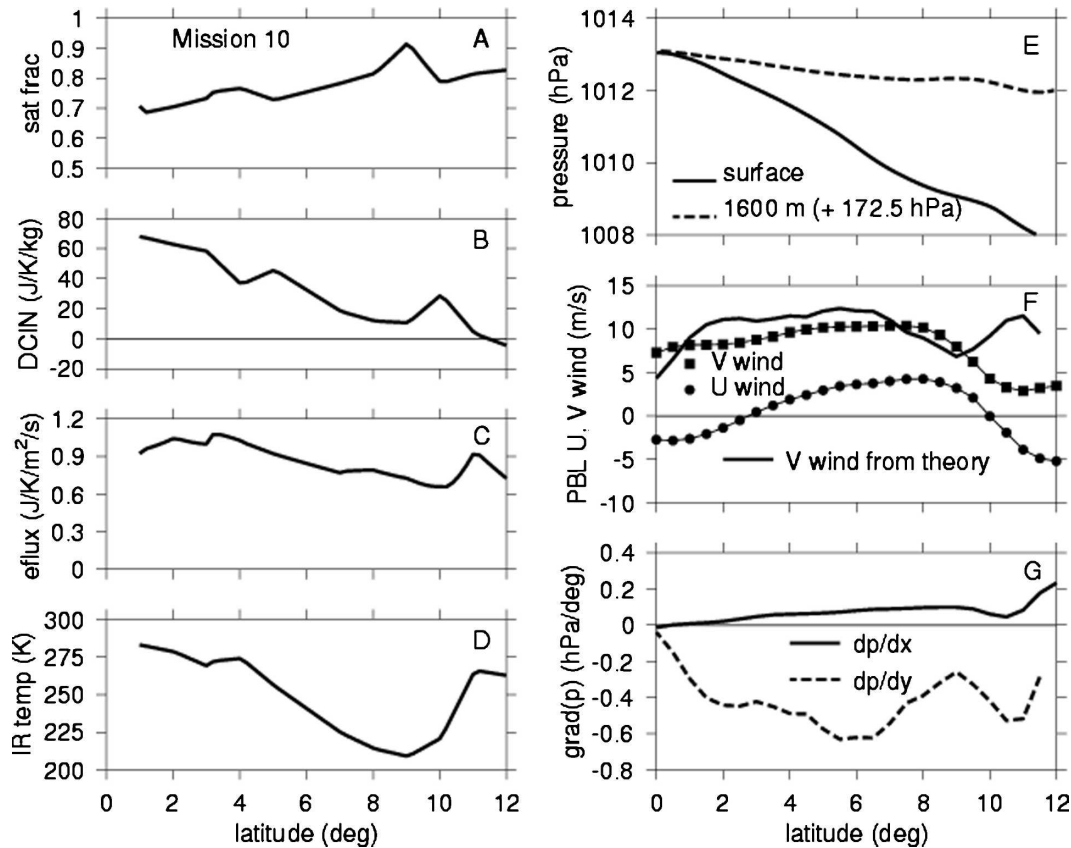


FIG. 12. Various quantities plotted as a function of latitude along 95°W from C-130 mission 10 (23 Sep 2001, day 266). (a) Saturation fraction below 480 hPa from dropsondes. (b) DCIN from dropsondes. (c) Surface moist entropy flux estimated from dropsonde data. (d) Satellite infrared brightness temperature. (e) Pressure at the surface and 1600 m from in situ C-130 observations. (f) Observed boundary layer zonal and meridional wind (filled bullets and squares) and the predicted meridional wind. (g) Observed meridional pressure gradient and predicted zonal pressure gradient.

case, especially in the convective disturbance near 9°N. The deep convective inhibition north of 8°N is greater than the projected mean. However, the variance of CIN is likely to be larger than average, as is common in regions of deep convection, due to the interleaving of unstable and downdraft air. Thus, the tail of the distribution of deep convective inhibition may well be more unstable than average. The surface entropy fluxes are much stronger than in the mean case due to the stronger surface winds.

This case fits the pattern suggested above; namely, a negative pressure gradient aloft (due to hurricane Juliette) generates a strong southerly PBL flow with correspondingly enhanced surface fluxes. The free-tropospheric saturation fraction is large as well, so deep convection is favored thermodynamically.

2) SUPPRESSED CONDITIONS

Conditions were highly suppressed along 95°W on 2 October 2001 (mission 14, day 275). Figure 13 shows

that the low-level southerly flow on this date was largely confined to south of 6°N. North of this latitude the surface winds were light and variable. Deep convection was absent at the northern limit of the southerlies on this date. However, a shallow but strong return flow to the south is seen between 800 and 875 hPa, implying the existence of shallow ascent near 6°N.

The distribution of surface winds and infrared brightness temperature for this day are shown in Fig. 14. Curiously, the scenario here is similar to the case with active conditions in that a tropical storm (Lorena) sits to the west of the study area. This storm showed a surface inflow structure similar to that seen in Juliette (Fig. 11), the difference being that Lorena was considerably weaker and farther west than Juliette during the respective observation periods. Thus, unlike the active case, the 95°W line was out of the main inflow into Lorena. Some transient deep convection developed near 95°N, 12°N on this day, but was too weak to show up in the daily average presented in Fig. 14.

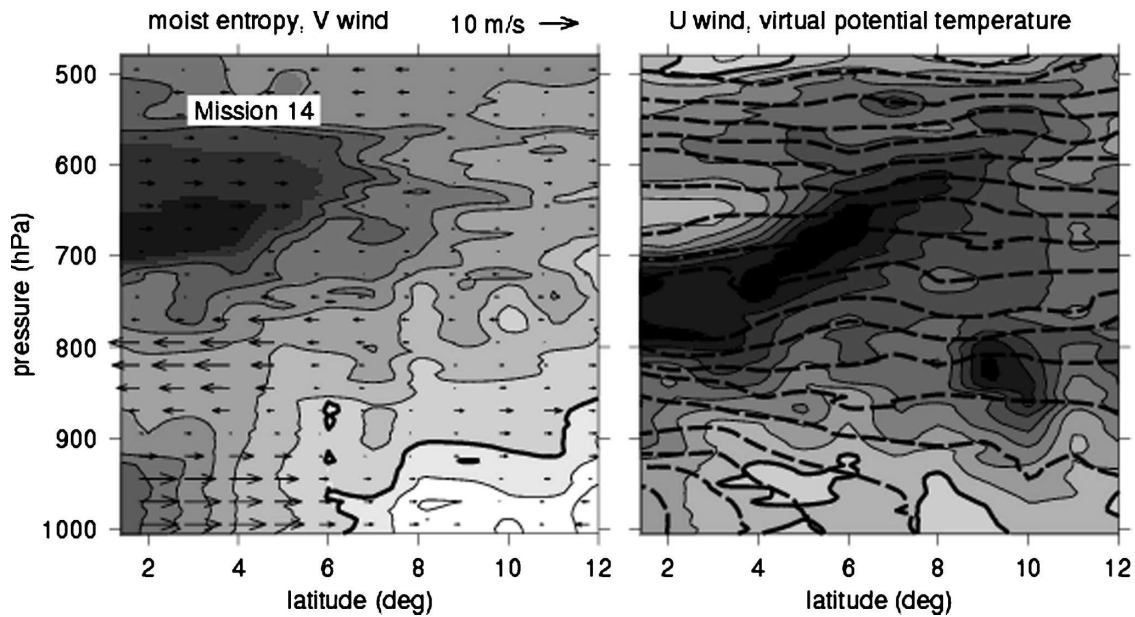


FIG. 13. As in Fig. 2, except for mission 14 (2 Oct 2001, day 275).

Figure 15 shows that MZB accurately predicted the meridional wind on this day. Meridional low-level convergence was predicted by MZB (and observed) in the range 4° – 6° N. No deep convection was in evidence at these latitudes. As noted above, shallow ascent occurred near 6° N in coincidence with the decrease of DCIN to zero. The low value of saturation fraction at this latitude may explain the lack of deep convection in this ascending region. The dropsonde sounding at 6° N shows stability (in the sense of CAPE) only slightly greater than that seen during mission 10 at 8° N. However, the low- to midtropospheric humidity is significantly less.

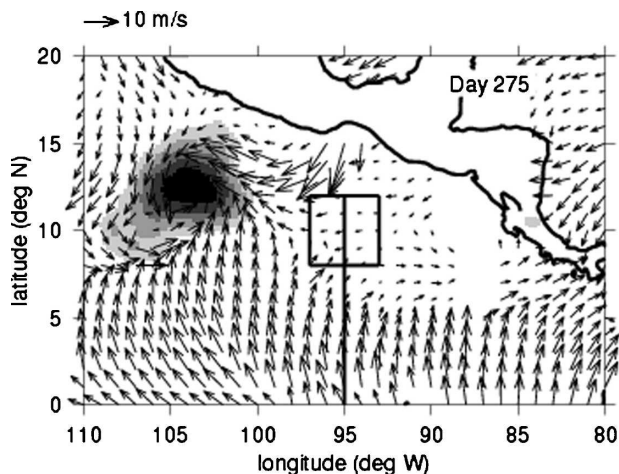


FIG. 14. As in Fig. 11, except for mission 14 (2 Oct 2001, day 275).

The saturation fraction north of 8° N is comparable to or greater than the project mean shown in Fig. 3, and DCIN in this region is actually negative. However, the surface winds are weak north of 6° N. Thus, the region north of 8° N is convectively unstable, but the instability is supported by only weak surface fluxes. BLQ thus predicts the observed weakness of convection in spite of the relatively moist and unstable conditions north of about 8° N.

Figure 15 reveals why the low-level southerly flow terminated at such a low latitude in this case. The 1600-m pressure is actually higher at 12° N than it is at the equator, and the surface pressure gradient is close to zero north of about 6° N as a result. Only isolated weak PBL westerlies exist during mission 14, as Fig. 13 shows. Aloft, strong easterlies prevail, in agreement with the meridional pressure gradient there.

6. Conclusions

We conclude that the extended Ekman balance theory of Stevens et al. (2002) as applied by McGauley et al. (2004) provides a good model of the southerly flow between the equator and the ITCZ in the eastern Pacific. However, at and north of the ITCZ, downdrafts associated with deep convection cause strong perturbations in the PBL momentum balance, often resulting in poor predictions by the model.

The PBL pressure gradient driving the above Ekman balance model results from a combination of SST gradient-induced effects and pressure gradients imposed

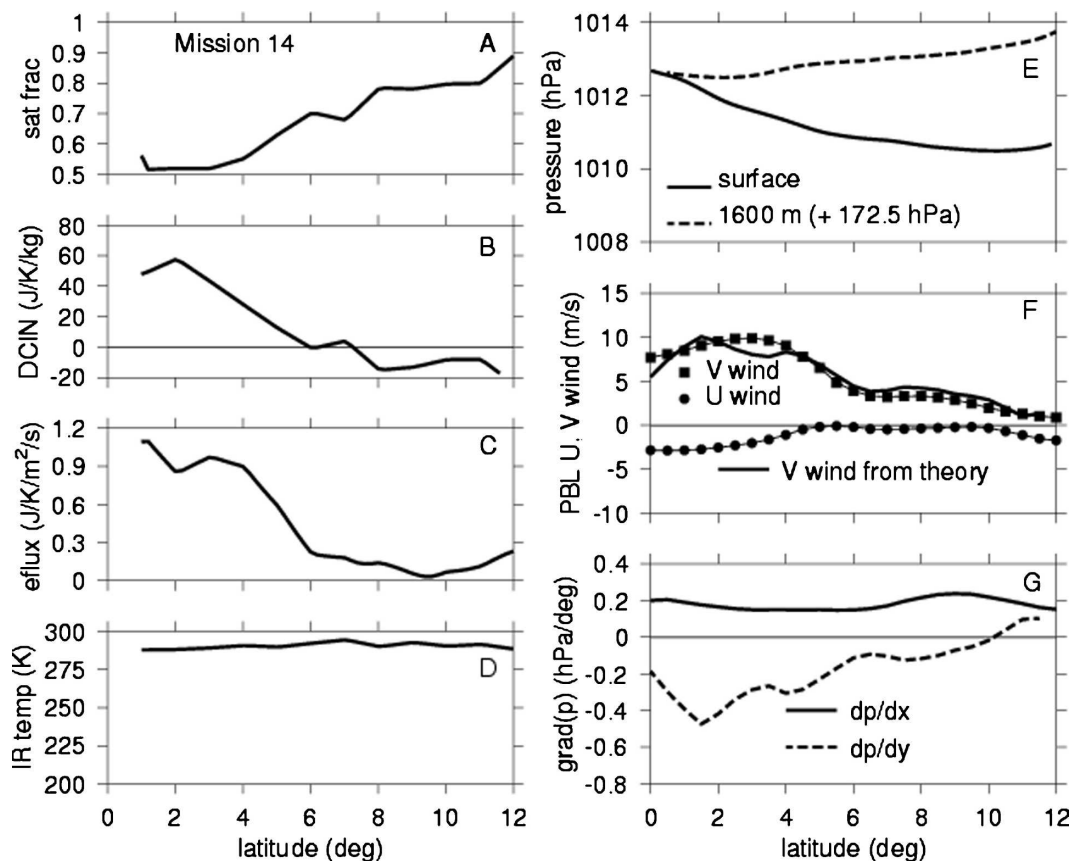


FIG. 15. As in Fig. 12, except for mission 14 (2 Oct 2001, day 275).

from above the boundary layer by disturbances such as easterly waves, tropical cyclones, and the Madden-Julian oscillation. Low pressure aloft to the north is associated with northward excursion of the low-level southerly flow.

When the southwesterlies extend to the north over warmer water, they produce enhanced surface fluxes in a region that normally experiences weak winds and correspondingly weak entropy fluxes. The enhanced fluxes support the development of widespread deep convection. This is the primary forcing mechanism for deep convection observed in the east Pacific ITCZ during the EPIC2001 field program.

The relative importance of convergence in the PBL and the surface moist entropy flux was evaluated using the budget of moist entropy in the PBL. Our results show that in the east Pacific ITCZ the surface moist entropy flux supplies on average more than twice as much entropy to convection as does PBL convergence. Furthermore, deep convection was more sensitive to the surface fluxes than to the convergence.

Observations during EPIC2001 showed that the east Pacific ITCZ stayed relatively moist during most of the

field program. Whether this is true over longer periods is uncertain. However, it appears to explain why variances in surface entropy fluxes were able to explain such a large fraction of the variance of deep convection during the project (see R03). As has recently been demonstrated by Sobel et al. (2004) and Bretherton et al. (2004), other regions exhibit much greater variance in deep convection attributable to variations in free tropospheric humidity.

Acknowledgments. This project would have been impossible without the hard work of the UCAR Joint Office for Scientific Support, NCAR's Research Aviation Facility, NOAA's Aircraft Operations Center, and the faculty and staff of the Centro de Ciencias de la Atmósfera at the Universidad Nacional Autónoma de México (CCA-UNAM). The Colorado State University staff on the ship *Ron Brown* did an excellent job of deploying radiosondes. Beverly Davis analyzed the GOES and SSM/I satellite data. Anonymous reviews made this paper significantly better. Thanks go to Jay Fein of the National Science Foundation (NSF) and Mike Patterson of NOAA's Office of Global Programs

(OGP) for their dedicated support of EPIC2001. NSF and NOAA directly supported the deployment of the two aircraft and the two ships. NOAA's Pacific Marine Environmental Laboratory, which maintains the TAO mooring array, deployed three extra buoys and enhanced the instrumentation on all the 95°W moorings for EPIC2001 with the support of NOAA/OGP. This work was sponsored by NSF Grants ATM-0082612, ATM-0352639, ATM-0082384, ATM-0002387, and Consejo Nacional de Ciencia y Tecnología (CONACyT) Grant 33319. The first author spent the academic year 2001–02 at CCA-UNAM in Mexico City with generous support from CONACyT. Special thanks go to Graciela Raga of CCA-UNAM for all the help on this project.

APPENDIX

Aircraft Pressure Measurements

In situ pressure measurements were used in combination with radar altimeter measurements to estimate pressures at fixed levels near the aircraft flight level for both aircraft using the hydrostatic equation in finite difference form:

$$\frac{p_a - p_l}{z_a - z_l} = -\frac{gp_a}{RT_a}, \quad (\text{A1})$$

where p_a and p_l are the pressure at the aircraft and fixed levels, z_a is the measured radar altitude of the aircraft, z_l is the altitude of the fixed level, g is the acceleration of gravity, R is the gas constant for air, and T_a is the temperature of the air at flight level. The difference between z_a and z_l is kept small enough (a few tens of meters) that virtual temperature effects and the variation of the right side of this equation with height are not important. The pressure at the fixed level p_l is easily solved.

Since the objective is to estimate horizontal pressure gradients at a fixed time, the diurnal cycle of pressure estimated from the TAO moorings is first subtracted from the in situ pressures. Hourly pressure data from all 95°W moorings during the period 1 September–15 October 2001 were used to produce a two-term fit to the pressure oscillation:

$$\Delta p = 0.4345 \cos[2\pi(t - 0.5124)] + 1.3340 \cos[4\pi(t - 0.1771)], \quad (\text{A2})$$

where the time t is in days and the pressure oscillation Δp is in hPa. This fits the mooring-averaged data to within 0.05 hPa, and the standard deviation between moorings is 0.1–0.2 hPa. Given the smallness of these deviations, we assume that the diurnal and semidiurnal

cycles are spatially uniform over the study area. The semidiurnal cycle is the major contributor here, and is due primarily to thermal tides in the thermosphere (Lindzen 1971; Hong and Lindzen 1976). Thus, its magnitude should be independent of height in the troposphere.

In mission 3 the P-3 flew outbound near 1900 m south to 5° and returned along the same track at the same elevation. The corrected pressure at this level matches between the outbound and inbound legs to within 0.3 hPa. Furthermore, the variation of the difference with latitude is weak, which indicates that rather sensitive estimates of horizontal pressure gradients at fixed time can be made with confidence using this technique.

REFERENCES

- Back, L. E., and C. S. Bretherton, 2005: The relationship between wind speed and precipitation in the Pacific ITCZ. *J. Climate*, **18**, 4317–4328.
- Battisti, D. S., E. S. Sarachik, and A. C. Hirst, 1999: A consistent model for the large-scale steady surface atmospheric circulation in the Tropics. *J. Climate*, **12**, 2956–2964.
- Bretherton, C. S., M. E. Peters, and L. E. Back, 2004: Relationships between water vapor path and precipitation over the tropical oceans. *J. Climate*, **17**, 1517–1528.
- Freilich, D., G. Long, and M. W. Spencer, 1994: SeaWinds: A scanning scatterometer for ADEOS II: Science overview. *Proc. Int. Geoscience Remote Sensing Symp.*, Vol. II, IEEE 94CH3378-7, Pasadena, CA, 960–963.
- Grabowski, W. W., 2003: MJO-like coherent structures: Sensitivity simulations using the cloud-resolving convection parameterization (CRCP). *J. Atmos. Sci.*, **60**, 847–864.
- Hayes, S. P., L. J. Mangum, J. Picaut, A. Sumi, and K. Takeuchi, 1991: TOGA-TAO: A moored array for real-time measurements in the tropical Pacific Ocean. *Bull. Amer. Meteor. Soc.*, **72**, 339–347.
- Hong, S.-S., and R. S. Lindzen, 1976: Solar semidiurnal tide in the thermosphere. *J. Atmos. Sci.*, **33**, 135–153.
- Jorgensen, D. P., T. Matejka, and J. D. DuGranrut, 1996: Multi-beam techniques for deriving wind fields from airborne Doppler radars. *Meteor. Atmos. Phys.*, **59**, 83–104.
- , T. R. Shepherd, and A. S. Goldstein, 2000: A dual-pulse repetition frequency scheme for mitigating velocity ambiguities of the NOAA P-3 airborne Doppler radar. *J. Atmos. Oceanic Technol.*, **17**, 585–594.
- Liebmann, B., and C. A. Smith, 1996: Description of a complete (interpolated) outgoing longwave radiation dataset. *Bull. Amer. Meteor. Soc.*, **77**, 1275–1277.
- Lindzen, R. S., 1971: Internal gravity waves in atmospheres with realistic dissipation and temperature: Part III. Daily variations in the thermosphere. *Geophys. Fluid Dyn.*, **1**, 303–355.
- , and S. Nigam, 1987: On the role of sea surface temperature gradients in forcing low-level winds and convergence in the Tropics. *J. Atmos. Sci.*, **44**, 2418–2436.
- Lucas, C., E. J. Zipser, and B. S. Ferrier, 2000: Sensitivity of tropical west Pacific oceanic squall lines to tropospheric wind and moisture profiles. *J. Atmos. Sci.*, **57**, 2351–2373.
- Madden, R. A., and P. R. Julian, 1994: Observations of the 40–50

- day tropical oscillation—A review. *Mon. Wea. Rev.*, **122**, 814–837.
- McGauley, M., C. Zhang, and N. Bond, 2004: Large-scale characteristics of the atmospheric boundary layer in the eastern Pacific cold tongue–ITCZ region. *J. Climate*, **17**, 3907–3920.
- McPhaden, M. J., 1995: The Tropical Atmosphere Ocean array is completed. *Bull. Amer. Meteor. Soc.*, **76**, 739–741.
- Raymond, D. J., 1995: Regulation of moist convection over the west Pacific warm pool. *J. Atmos. Sci.*, **52**, 3945–3959.
- , and X. Zeng, 2005: Modeling tropical atmospheric convection in the context of the weak temperature gradient approximation. *Quart. J. Roy. Meteor. Soc.*, **131**, 1301–1320.
- , G. B. Raga, C. S. Bretherton, J. Molinari, C. López-Carrillo, and Ž. Fuchs, 2003: Convective forcing in the intertropical convergence zone of the eastern Pacific. *J. Atmos. Sci.*, **60**, 2064–2082.
- , and Coauthors, 2004: EPIC2001 and the coupled ocean–atmosphere system of the tropical east Pacific. *Bull. Amer. Meteor. Soc.*, **85**, 1341–1354.
- Reynolds, R. W., 1988: A real-time global sea surface temperature analysis. *J. Climate*, **1**, 75–86.
- , and D. C. Marsico, 1993: An improved real-time global sea surface temperature analysis. *J. Climate*, **6**, 114–119.
- Riehl, H., T. C. Yeh, J. S. Malkus, and N. E. La Seur, 1951: The north-east trade of the Pacific Ocean. *Quart. J. Roy. Meteor. Soc.*, **77**, 598–626.
- Sherwood, S. C., 1999: Convective precursors and predictability in the tropical western Pacific. *Mon. Wea. Rev.*, **127**, 2977–2991.
- Sobel, A. H., S. E. Yuter, C. S. Bretherton, and G. N. Kiladis, 2004: Large-scale meteorology and deep convection during TRMM KWAJEX. *Mon. Wea. Rev.*, **132**, 422–444.
- Stevens, B., J. Duan, J. C. McWilliams, M. Munnich, and J. D. Neelin, 2002: Entrainment, Rayleigh friction, and boundary layer winds over the tropical Pacific. *J. Climate*, **15**, 30–44.
- Tomas, R. A., and P. J. Webster, 1997: The role of inertial instability in determining the location and strength of near-equatorial convection. *Quart. J. Roy. Meteor. Soc.*, **123**, 1445–1482.
- , J. R. Holton, and P. J. Webster, 1999: The influence of cross-equatorial pressure gradients on the location of near-equatorial convection. *Quart. J. Roy. Meteor. Soc.*, **125**, 1107–1127.
- Tompkins, A. M., 2001: Organization of tropical convection in low vertical wind shears: The role of water vapor. *J. Atmos. Sci.*, **58**, 529–545.
- Yin, B., and B. A. Albrecht, 2000: Spatial variability of atmospheric boundary layer structure over the eastern equatorial Pacific. *J. Climate*, **13**, 1574–1592.
- Zhang, C., M. McGauley, and N. A. Bond, 2004: Shallow meridional circulation in the tropical eastern Pacific. *J. Climate*, **17**, 133–139.